Supporting Information

On the Reliability of Acquiring Molecular Junction Parameters by Lorentzian Fitting of I/V curves

Vincent Delmas, Valentin Diez-Cabanes, Colin van Dyck, Elke Scheer, Karine Costuas*, Jérôme Cornil*

Table of contents

1. Electrode | molecule | electrode representation
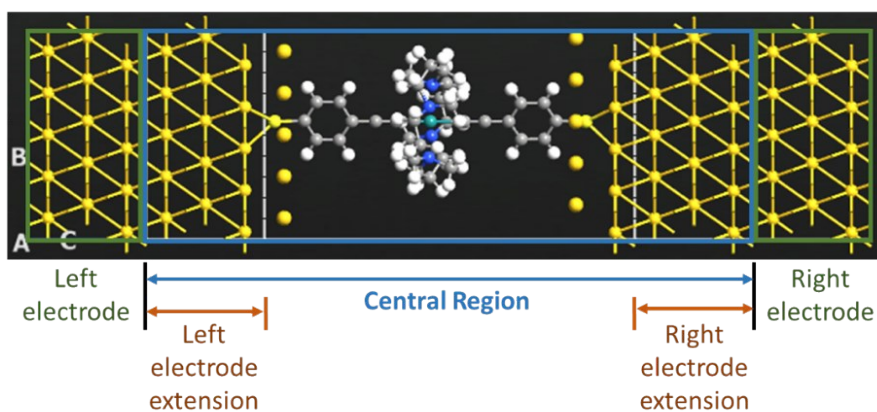
Figure S1. Representation of the junction (electrode | molecule | electrode) built with ATK.[1] The sulfur atoms are anchored in the hollow position on the (111) surface of gold. We use ghost atoms on top of the gold surface (represented by the yellow spheres) to obtain a better electronic description of the surface and obtain a more accurate value of the work function of the (111) gold surface.[2]

2. DFT+NEGF - ATK - Details of calculations[1]

The unit cell of our system was not optimized.

- Numerical details:
    - The k points sampling in the (a, b, c) directions: [5;5;50]
    - Density mesh cutoff: 200 Rydberg
    - Iteration accuracy tolerance: 10^{-5} Hartree
    - Poisson solver: FF2D (Fast Fourier 2D)
    - Semi-circle contour:
        - Integral lower bound: 1.5 Hartree
        - 30 circle points
- Basis set:
    - Ru, N, C, H: Double zeta + polarization
    - Au: Single zeta + polarization

- Exchange-Correlation functional:
    - GGA – RevPBE
- Molecular junction pattern:
    - [ABC]ABC-molecule-CABC[ABC]
- [ABC] Au (111) unit cell vectors:
    - a = [14.419, 0.0, 0.0] Å
    - b = [-7.209, 12.480, 0.0] Å
    - c = [0.0, 0.0, 7.064] Å

3. Calculation of the Seebeck coefficient

In the linear regime conditions,[3] Eq. 3 can be simplified into:

$$I = e^2 L_0 \Delta V + e L_1 \frac{\Delta T}{T}$$

<div align="right">Eq. S1</div>

$$L_n = -\frac{2e}{h} \int \tau(E,V)\ (E - \mu)^n\ \frac{df}{dE}\ dE$$

<div align="right">Eq. S2</div>

By setting the current I equal to 0, which is required for the calculation/measurement of S, i.e. Eq $S_1 = 0$, the following expression for ΔV can be deduced:

$$e^2 L_0 \Delta V = -\ e L_1 \frac{\Delta T}{T}\ \Leftrightarrow \Delta V = -\frac{1}{eT}\frac{L_1}{L_0}\Delta T$$

<div align="right">Eq. S3</div>

With $S = -\dfrac{\Delta V}{\Delta T}$, we get:

$$S = -\frac{1}{T}\frac{L_1}{L_0}$$

<div align="right">Eq. S4</div>

4. Transmission and I/V curve fitting methods

The fittings were performed using NumPy, SciPy and Sklearn modules in Python applying the Eq. 3 for the current I and Eq. 2 for the transmission $\tau(E)$. We used the SciPy and NumPy module for the curve fitting using the Levenberg-Marquardt (LM) algorithm, and Sklearn for the R^2 implementation. For the fitting of the $\tau(E)$ functions, we use only the part between the maximum peak and the Fermi energy.

5. Molecular orbital diagram of *trans*-Ru(TMA)(C≡C-C$_6$H$_5$)$_2$ and transmission properties of the molecular junction
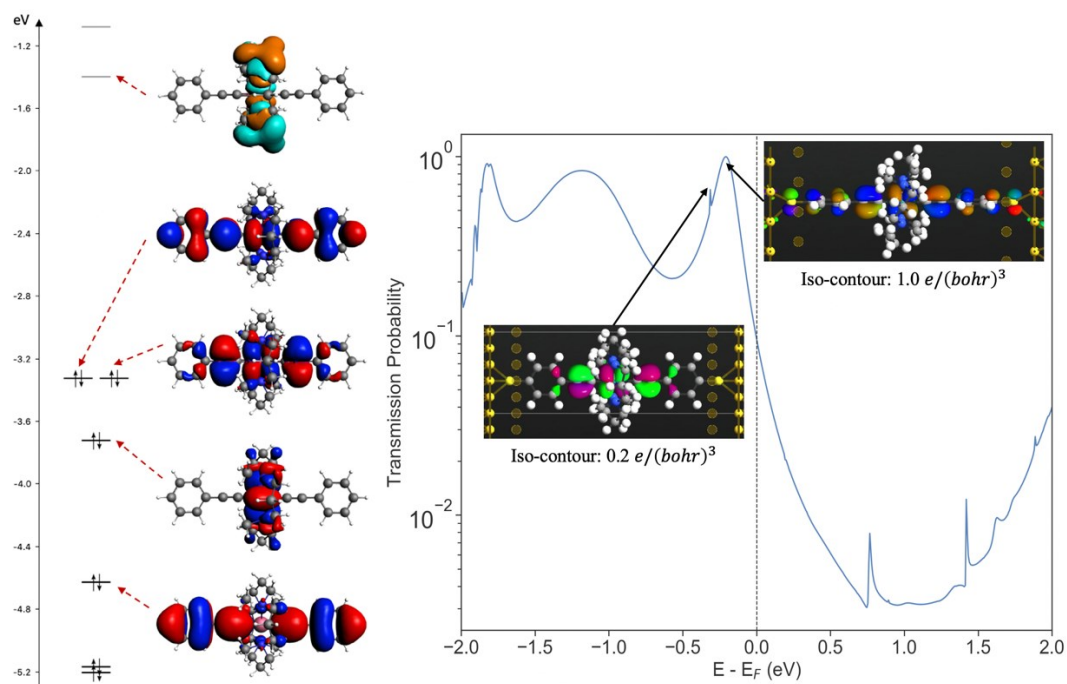
Figure S2. Left: Molecular orbital diagram of the isolated molecule *trans*-Ru(TMA)(C≡C-C$_6$H$_5$)$_2$; Iso-contour plots of the highest occupied molecular orbitals (MO).[4-6] Right: Transmission spectrum of the molecular junction at 0 V; representation of two transmission eigenstates for the two maxima of interest.[6]

6. Transmission spectra
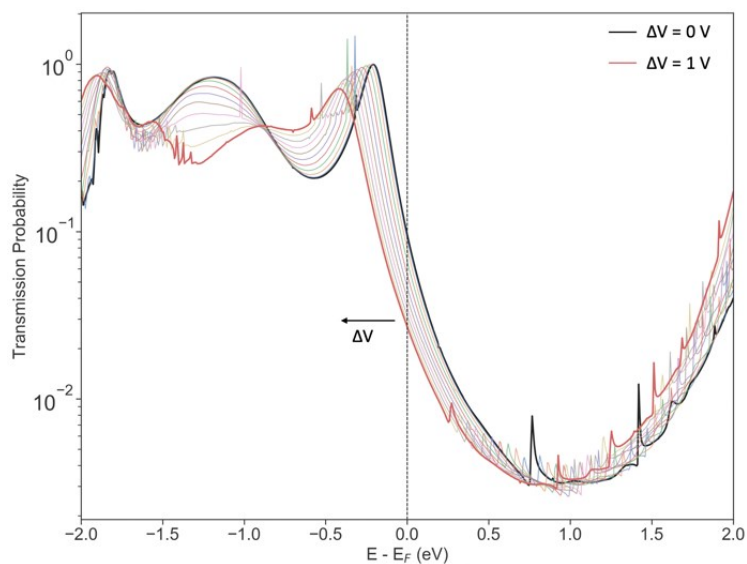
Figure S3. Calculated transmission spectra of the Au | *trans*-Ru(TMA)(C≡C-C$_6$H$_4$S)$_2$ | Au junction at biases ranging from 0 to 1 V by steps of 0.1 V.
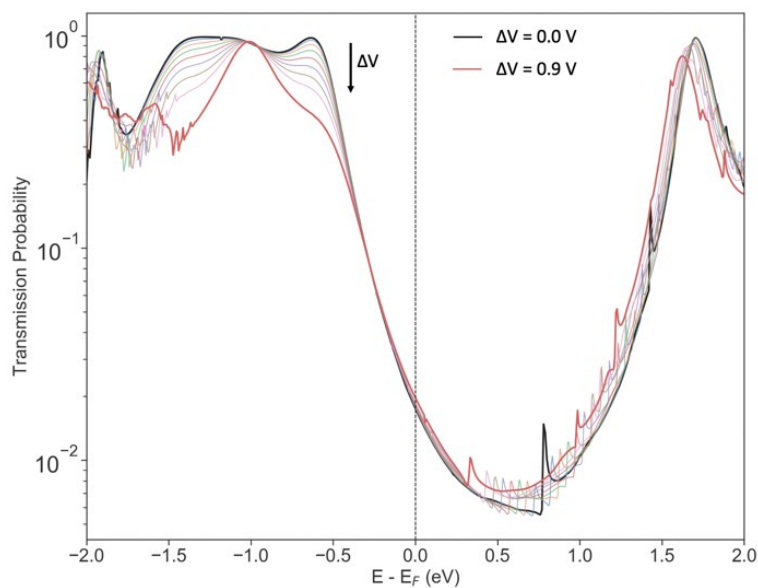
Figure S4. Calculated transmission spectra of an Au | oligo(phenylene-ethynylene) | Au junction at biases ranging from 0 to 0.9 V by steps of 0.1 V, as obtained using the same computational approach.

7. Molecular characteristics of the Au | *trans*-Ru(TMA)(C≡C-C$_6$H$_4$S)$_2$ | Au junction

Table S1. Γ_τ (eV), $\epsilon_{0-\tau}$ (eV), S (μV/K) and G (G/G$_0$) obtained by application of the single-level method to fit $\tau(E)$ at each applied voltage (V). The average values of the different parameters in the bias interval between 0 and 0.2 eV and between 0 and 1 V are the values reported in Table 1.

V	Γ_τ	$\varepsilon_{0-\tau}$	S_τ	G_τ/G_0
0.0	0.034	-0.214	88	0.114
0.1	0.034	-0.221	87	0.114
0.2	0.034	-0.234	83	0.116
0.3	0.035	-0.259	78	0.120
0.4	0.035	-0.281	72	0.127
0.5	0.036	-0.310	66	0.135
0.6	0.037	-0.337	60	0.143
0.7	0.039	-0.358	56	0.151
0.8	0.040	-0.381	52	0.156
0.9	0.043	-0.402	50	0.159
1.0	0.046	-0.429	49	0.159
[0.0 - 0.2] av.	0.034	-0.223	86	0.115
[0.0 - 1.0] av.	0.038	-0.311	67	0.136

Table S2. Percentage error of Γ (eV), ϵ_0 (eV), S (μV/K) and G/G_0 obtained by a) the fitting of the I/V curve ($_{I/V}$) and b) by adding G and S to the fitting procedure ($_{"G+S"}$) (see Table 1) with respect to the reference values Γ_τ, $\epsilon_{0-\tau}$, S_τ, G_τ/G_0 respectively.

a)

R^2 I/V curve fit	Voltage range (V)	$\Gamma_{I/V}$ % error	$\epsilon_{0-I/V}$ % error	$S_{I/V}$ % error	$G_{I/V}/G_0$ % error
0.997	[0.0 - 1.0]	340.0	177.1	77.8	5.1
1.000	[0.0 - 0.2]	208.4	164.4	73.7	0.9
1.000	[0.0 - 0.1]	398.6	335.6	84.2	0.0

b)

$\Gamma_{"G+S"}$ % error	$\epsilon_{0-"G+S"}$ % error	$S_{"G+S"}$ % error	$G_{"G+S"}/G_0$ % error
8.6	13.2	0.9	0.9

Table S3. Number of retained values of the (Γ, ϵ_0) couples for different numbers of initial couple values and for different threshold values (from 2 to 15 %). The retained values represent the number of couples that satisfies a given threshold. σ is the standard deviation, as implemented in the numpy module in python.

ϵ_0 range (eV)	Γ range (eV)	Initial number (#) of couples ($\#\epsilon_0 \times \#\Gamma$)	Threshold (%)	Number of retained values	$\bar{\epsilon}_0$ in eV [σ]	$\bar{\Gamma}$ in eV [σ]
-2.0 to 0.0	0.01 to 0.1	10 201 (101×101)	4	0	NaN	NaN
		40 401 (201×201)	4	5	-0.188 [4.10^{-3}]	30.6 [0.8]
		251 001 (501×501)	2	8	-0.186 [2.10^{-3}]	30.2 [0.5]
			4	24	-0.186 [4.10^{-3}]	30.2 [0.7]
			6	55	-0.187 [5.10^{-3}]	30.3 [1.1]
			8	95	-0.187 [7.10^{-3}]	30.3 [1.4]
			10	150	-0.188 [9.10^{-3}]	30.5 [1.8]
			12	218	-0.188 [11.10^{-3}]	30.6 [2.2]
			15	350	-0.190 [14.10^{-3}]	30.8 [2.7]
		1 002 001 (1001×1001)	4	95	-0.186 [4.10^{-3}]	30.2 [0.7]
		4 004 001 (2001×2001)	4	382	-0.186 [4.10^{-3}]	30.2 [0.7]

8. Main lines of the algorithm used to execute the "G+S" method

G_{ref} and S_{ref} of reference are given as target values as well as the associated threshold value (i.e., acceptable margin error). The initialization step is done by setting the energy domains of Γ and ϵ_0 couples and the number of possible values for each parameter. An energy range is also fixed for the calculation of the transmission (for example, in python, using the numpy and "linspace" to create evenly spaced values):

$Energy = numpy.linspace(-2, 2, size)$

$\Gamma = numpy.linspace(0.01, 0.1, sample\_size)$

$\epsilon_0 = numpy.linspace(-2, 0, sample\_size)$

The first derivative of the Fermi-Dirac distribution of the reservoirs/electrodes is defined and calculated, with k the Boltzmann constant and T the temperature (T = 300 K in the paper), as follows:

$$\frac{df}{dE} = - \frac{exp^{\frac{Energy}{k.T}}}{k.T\left(exp^{\frac{Energy}{k.T}} + 1\right)^2}$$

Then, for each Γ and for each ϵ_0 (double "for" loop):

- Calculation of the transmission:

$$\tau_E = \frac{4\Gamma^2}{(Energy - \epsilon_0)^2 + 4\Gamma^2}$$

- Calculation of the function to be integrated for the thermoelectrics data (in the linear regime):

$$int_{L_0} = \tau_E . -\frac{df}{dE}$$

$$int_{L_1} = \tau_E\left(-\frac{df}{dE}.Energy\right)$$

- Calculation of a numerical estimation of the integrals using Simpson's rule:

$$L_0 = simps(int_{L_0}, Energy)$$

$$L_1 = simps(int_{L_1}, Energy)$$

- Calculation of the Seebeck S coefficient and conductance G (G/G$_0$):

$$S = -\left(\frac{1}{T}\frac{L_1}{L_0}\right)$$

$$G = L_0$$

- Calculations of the Seebeck and conductance deviations between the values obtained from this (Γ, ϵ_0) couple and the reference values:

$$G_{error} = |G_{ref} - G|$$

$$G_{error_{percentage}} = \left(\frac{G_{error}}{G_{ref}}\right) * 100$$

$$S_{error} = |S_{ref} - S|$$

$$S_{error\,percentage} = \left(\frac{S_{error}}{S_{ref}}\right) * 100$$

- Check whether the error percentage is below or equal to the chosen threshold. If true, then keep this (Γ, ϵ_0) couple else the couple is rejected. The procedure is looped until all (Γ, ϵ_0) couples have been evaluated.

- Results: mean value of all retained couples + statistical data (variance, standard deviation)

9. Evaluation of Γ_τ and $\varepsilon_{0-\tau}$ parameters
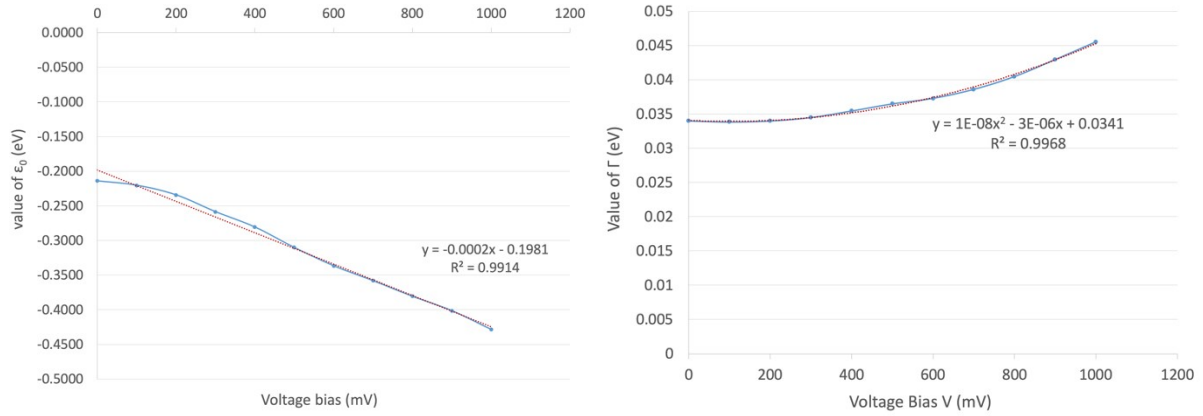
Figure S5. Evolution of $\varepsilon_{0-\tau}$, and Γ_τ (in eV) as a function of the applied bias V (in mV) based on the fitting of the transmission peak.
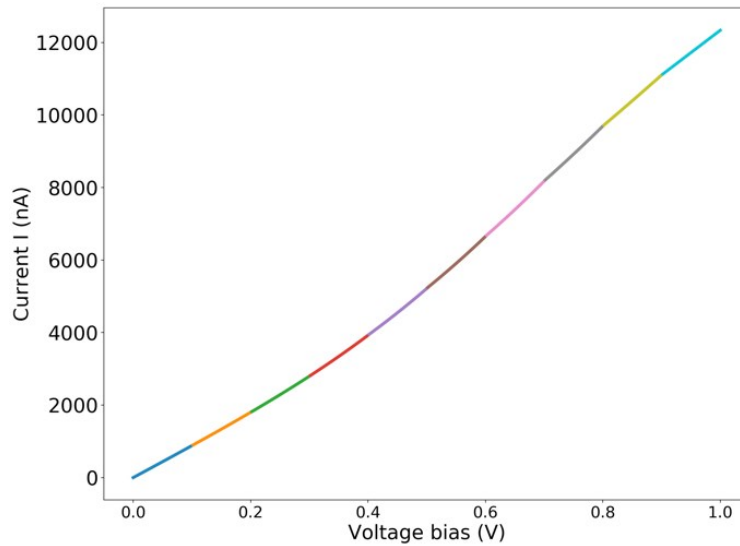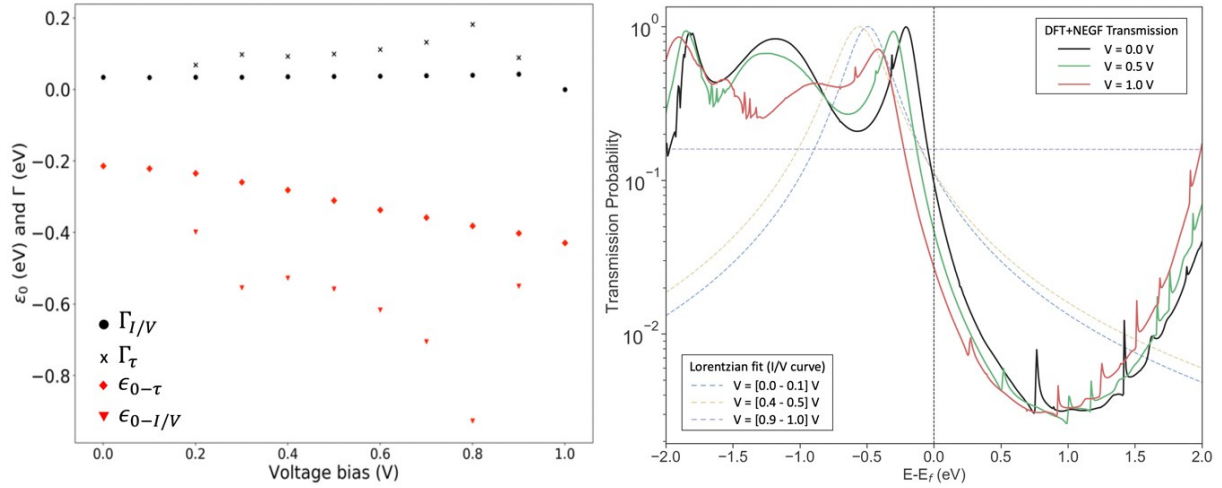
Figure S6. Top: visualization by color segment of the 100 mV parts of the I/V curve used for the integration to extract $\Gamma_{I/V}$ and $\varepsilon_{0\text{-}I/V}$; Bottom left: plot of the resulting $\Gamma_{I/V}$, $\varepsilon_{0\text{-}I/V}$ values as a function of the lower value of the bias voltage range. Bottom right: representation of the Lorentzian curves constructed using the previous results for three voltage ranges (the fit did not converge in the range $V = [0.9 - 1.0]$ V). The DFT+NEGF calculated transmissions at comparable voltages are depicted as solid lines for comparison.
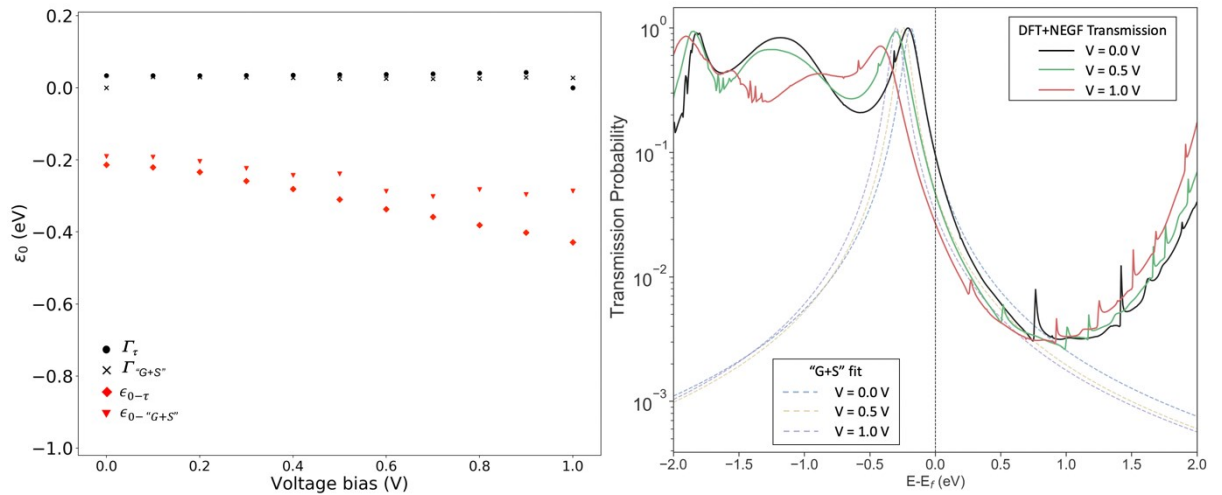
Figure S7. Left: plot of $\Gamma_{"G+S"}$ and $\varepsilon_{0\text{-}"G+S"}$ values calculated when including in the fit the conductance G from the relation G = I/V and the Seebeck S at each voltage. Bottom right: representation of the Lorentzian curves constructed using the previous results for three voltage ranges. The DFT+NEGF calculated transmissions at comparable voltages are shown in solid lines for comparison.

Table S4 – The experimental G and S values, G_{exp}/G_0 and S_{exp}, are extracted from reference 8 for three different gold |molecule| gold junctions: bi-phenyl and tri-phenyl (with thiol anchoring) and bipyridine (N-gold coordination). The value of $\varepsilon_{0\text{-theo}}$ is taken from the same article and corresponds to calculations performed at the DFT+Σ level. The values "I/V" and "G+S" are obtained by applying the procedures described in the main text to the experimental data (I/V curves, G_{exp}/G_0 and S_{exp}). Interestingly, the "G+S" method in green gives results closer to the experimental data (in blue) and closer to $\varepsilon_{0\text{-theo}}$ for the tri-phenyl and bi-pyridine systems. For the bi-phenyl case, the system can be well described with the fitting of the I/V curve only, and give similar results as the "G+S" method, pointing to a quasi-lorentzian shape of the transmission, in agreement with computational studies published in the same article.

Junction	S_{exp}	G_{exp}/G_0	$\varepsilon_{0\text{-theo}}$	$S_{I/V}$	$G_{I/V}/G_0$	$\varepsilon_{0\text{-I/V}}$	$\Gamma_{I/V}$	S_{G+S}	G_{G+S}/G_0	$\varepsilon_{0\text{-G+S}}$	Γ_{G+S}
bi-phenyl	13	0.0049	-1.5	13	0.0051	-1.184	0.042	13	0.0052	-1.13	0.039
tri-phenyl	15.7	1.65E-4	-1.25	27	1.69E-4	-0.57	0.003	16	1.68E-4	-0.93	0.006
bi-pyridine	-6.9	0.0011	2.0	-22.5	0.0012	0.67	0.011	-6.9	0.0011	2.1	0.035

10. References

(1) a) S. Smidstrup et *al. J. Phys.: Condens. Matter* 2020, **32**, 015901. b) M. Brandbyge, J. L. Mozos, P. Ordejón, J. Taylor and K. Stokbro *Phys. Rev. B* 2002**, 65**, 165401. c) S. Smidstrup, D. Stradi, J. Wellendorff, P. A. Khomyakov, U. G. Vej-Hansen, M-E. Lee, T. Ghosh, E. Jónsson, H. Jónsson and K. Stokbro, *Phys. Rev.* 2017, **B96**, 195309. d) QuantumATK Q-2019.12 Synopsys (https://www.synopsys.com/silicon/quantumatk.html).

(2) S. Smidstrup, D. Stradi, J. Wellendorff, P. A. Khomyakov, U. G. Vej-Hansen, M.-E. Lee, T. Ghosh, E. Jónsson, H. Jónsson, and K. Stokbro, *Physical Review B*, 2017**, 96** (19), 195309.

(3) G. D. Mahan, *Many-Particle Physics*, 3rd ed.; Physics of solids and liquids; *Kluwer Academic/Plenum Publishers:* New York, 2000.

(4) Calculations and MO plots were obtained using ADF **2019**; Slater basis set: TZ2P, small frozen core; Functional revPBE; Iso-contours: ± 0.01 (e/bohr^{-3})$^{-1/2}$.

(5) G. te Velde, F. M. Bickelhaupt, E. J. Baerends, C. Fonseca Guerra, S. J. A. van Gisbergen, J. G. Snijders and T. Ziegler, *J. Comput. Chem.*, 2001, **22**, 931.

(6) ADF **2019**, SCM, Theoretical Chemistry, Vrije Universiteit, Amsterdam, The Netherlands, http://www.scm.com.

(7) M. Paulsson and M. Brandbyge, *Phys. Rev. B*, 2007, **76**, 115117.

(8) L. Cui, R. Miao, K. Wang, D. Thompson, L. A. Zotti, J. C. Cuevas, E. Meyhofer and P. Reddy, *Nature Nanotechnology* 2018, **13**, 122–127.